
Article:
Wang, J.B., Taylor, B., Sun, Z.G. et al. (1 more author) (2007) Experimental characterization of a supercapacitor-based electrical torque-boost system for downsized ICE vehicles. IEEE Transactions on Vehicular Technology, 56 (6 (par). pp. 3674-3681. ISSN 0018 9545

https://doi.org/10.1109/TVT.2007.901885

Experimental Characterization of a Supercapacitor-Based Electrical Torque-Boost System for Downsized ICE Vehicles

Jiabin Wang, *Senior Member, IEEE*, Ben Taylor, Zhigang Sun, and David Howe

***Abstract*—The need to improve fuel economy and reduce the emission of CO_2 and other harmful pollution from internal-combustion-engine vehicles has led to engine downsizing. However, downsized turbocharged engines exhibit a relatively low torque capability at low engine speeds. To overcome this problem, an electrical torque boost may be employed while accelerating and changing gear and to facilitate energy recovery during regenerative braking. This paper describes the operational requirements of a supercapacitor-based torque-boost system, outlines the design and sizing of the electrical drive-train components, and presents experimental characterization of a demonstrator system.**

***Index Terms*—Electric torque boost, hybrid drive train, internal-combustion-engine (ICE) vehicles, permanent-magnet machine, supercapacitor.**

I. Introduction

AMID GROWING concerns over the greenhouse effect, measures to reduce CO_2 emissions are being promoted worldwide. However, it is widely accepted that a significant reduction will only be achieved through technological advances in the automotive sector. This has led to significant development in hybridization of vehicle power trains [1]–[3] via series, parallel, and series–parallel formats [4], [5]. One effective approach is engine downsizing, since a downsized internal combustion engine (ICE), which has high specific power by turbocharging (TC), has the potential to reduce fuel consumption by ∼30%, as compared to that of a naturally aspirated (NA) ICE with ∼65% higher displacement. However, TC ICEs exhibit a relatively low-torque capability at low engine speeds, as shown in Fig. 1, which compares the torque–speed characteristic of a 3l NA ICE with that of a 1.8l TC ICE. This results in an unacceptable drive-away and acceleration performance.

However, the low-speed torque deficit may be overcome by employing an electrical machine, supplied from an auxiliary supercapacitor energy-storage system, to provide a torque boost at low engine speeds [6], as shown in Figs. 1 and 2, from which it will be shown that the maximum boost torque of 132 N · m and the maximum boost power of 18.65 kW are required at engine speeds of 1069 and 1704 r/min, respectively. The supercapacitor may be recharged either by a regeneration from the electrical machine, when the engine speed is sufficiently high or vehicle kinetic energy is being recovered during braking, or by the use of energy stored in the battery, via the dc/dc converter. The latter may be necessary if the vehicle is not used for protracted periods when the supercapacitor unit may become discharged. However, since it only needs to provide power for recharging the supercapacitor and for normal operations, its size can be significantly smaller than that in the conventional vehicle. In the present system, a 40-A · h (480 W · h) battery is used. It will also be noted that, since the cranking torque which is required for the downsized ICE (∼140 N · m) is compatible with the peak torque-boost requirement, the torque-boost motor is also used to start the engine, and a separate cranking motor is not needed.

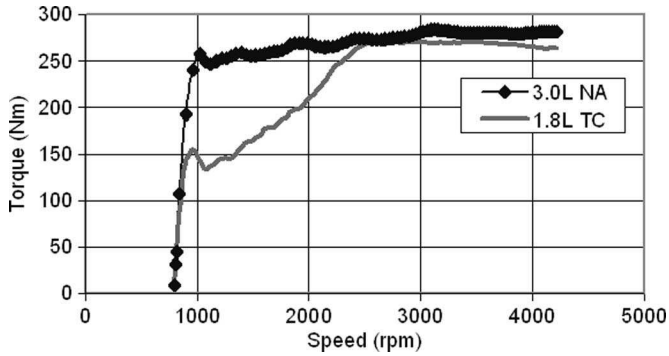

Fig. 1. Torque–speed characteristics of 3l NA and 1.8l TC engines and torque-boost machine (courtesy of FEV, Germany).

Since the torque boosting is only required at low engine speeds and the average power rating of the electric power components is significantly lower than that of conventional mild hybrid power-train configurations, this form of power-train configuration becomes particularly attractive to low-cost applications.

II. Sizing of Torque-Boost Components

The torque boost is only required for short periods, when the engine speed is < 3000 r/min. The torque–speed characteristic in Fig. 1 merely defines the peak torque capability required of the electrical machine. Its continuous rating, the energy-storage capacity of the supercapacitors, and the total energy consumption are dependent on the vehicle-driving cycle. A reference drive-away cycle is defined in Fig. 3, in which the

Manuscript received September 20, 2006; revised January 9, 2007 and February 16, 2007. This work was supported by the European Commission and the project partners FEV, RWTH, SAFT, Valeo, Renault, and SEMELAB. The review of this paper was coordinated by Prof. M. Benbouzid.

The authors are with the Department of Electronic and Electrical Engineering, University of Sheffield, S10 2TN Sheffield, U.K. (e-mail: j.b.wang@sheffield.ac.uk).

Digital Object Identifier 10.1109/TVT.2007.901885

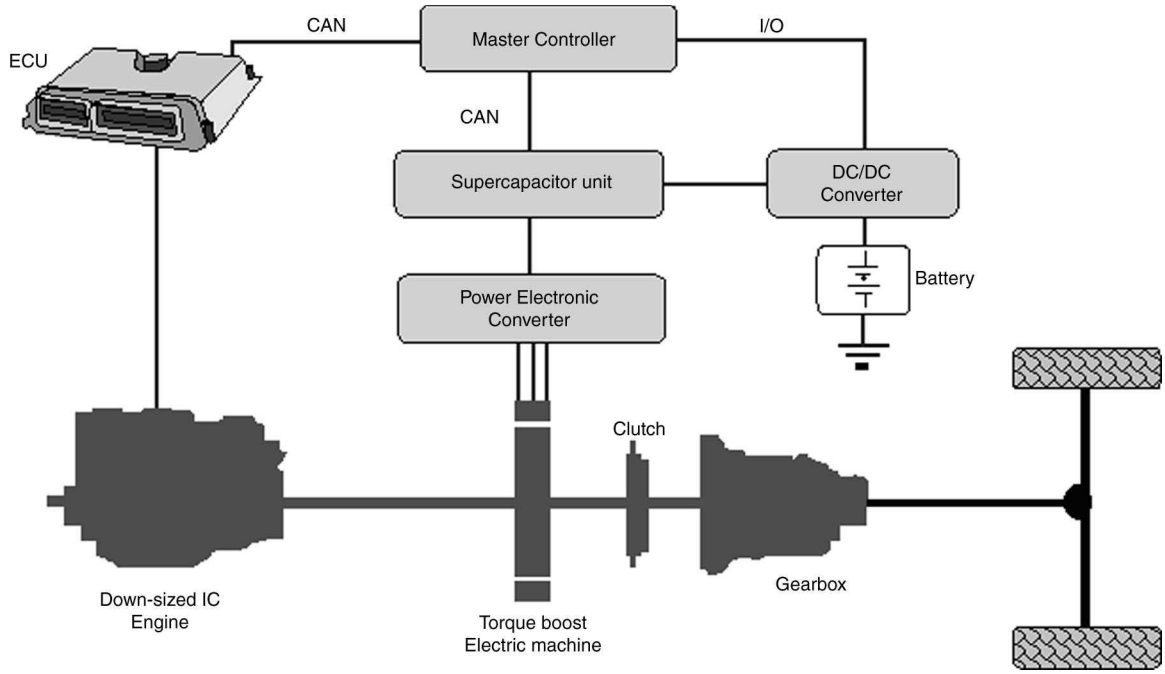

Fig. 2. Downsized ICE with supercapacitor-based torque boost (courtesy of EC EST project partners).

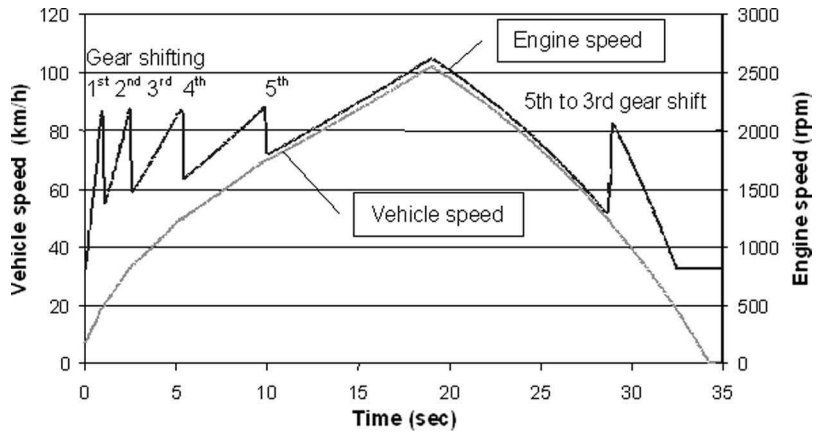

Fig. 3. Reference drive-away cycle (courtesy of FEV, Germany).

vehicle accelerates from standstill to 100 km/h in 18 s, with gear shifting at an engine speed of 2200 r/min, followed by deceleration to standstill in 16 s, with one gear change from fifth to third.

In order to examine the implication of the foregoing driving cycle on the sizing and thermal rating of the power-train components, a comprehensive simulation study has been carried out with detailed kinematic and dynamic models representing the vehicle and the electrical drive for the torque booster. Each component is represented by a macromodel that enables its main characteristics and losses to be deduced. During acceleration, the required electrical torque boost is determined according to the difference in the torque–speed characteristics of the 3.0l NA engine and the 1.8l TC downsized engine for a given vehicle speed and the gear which is engaged. Regenerative operation during braking enables kinetic energy to be recovered. Without loss of generality, an electrical torque-boost system based on a permanent-magnet brushless ac machine is assumed, although other machine technologies are also considered. Fig. 4 shows the variations of the required electrical torque, energy, and the supercapacitor voltage and current as functions of time over the reference driving cycle, as shown in Fig. 3. The relevant vehicle data are given in Table I. The supercapacitor unit comprises 36 3500-F 2.5-V series-connected supercapacitors, which are initially assumed to be fully charged. The maximum peak current of the supercapacitor is 750 A, and in the fully charged state, the supercapacitor unit has a peak power capability of 60 kW. However, its energy-storage capacity is relatively low ($\sim$390 kJ), which is equivalent to 110 $\mathrm{W}\cdot\mathrm{h}$. The amount of useful energy is even lower [295 kJ (82 $\mathrm{W}\cdot\mathrm{h}$)], since the minimum dc-link voltage for the motor drive is 45 V, and the undervoltage protection of the drive unit will inhibit power-electronic inverter operation.

As will be shown, the maximum energy consumption during the acceleration period is $\sim$150 kJ. However, this is fully

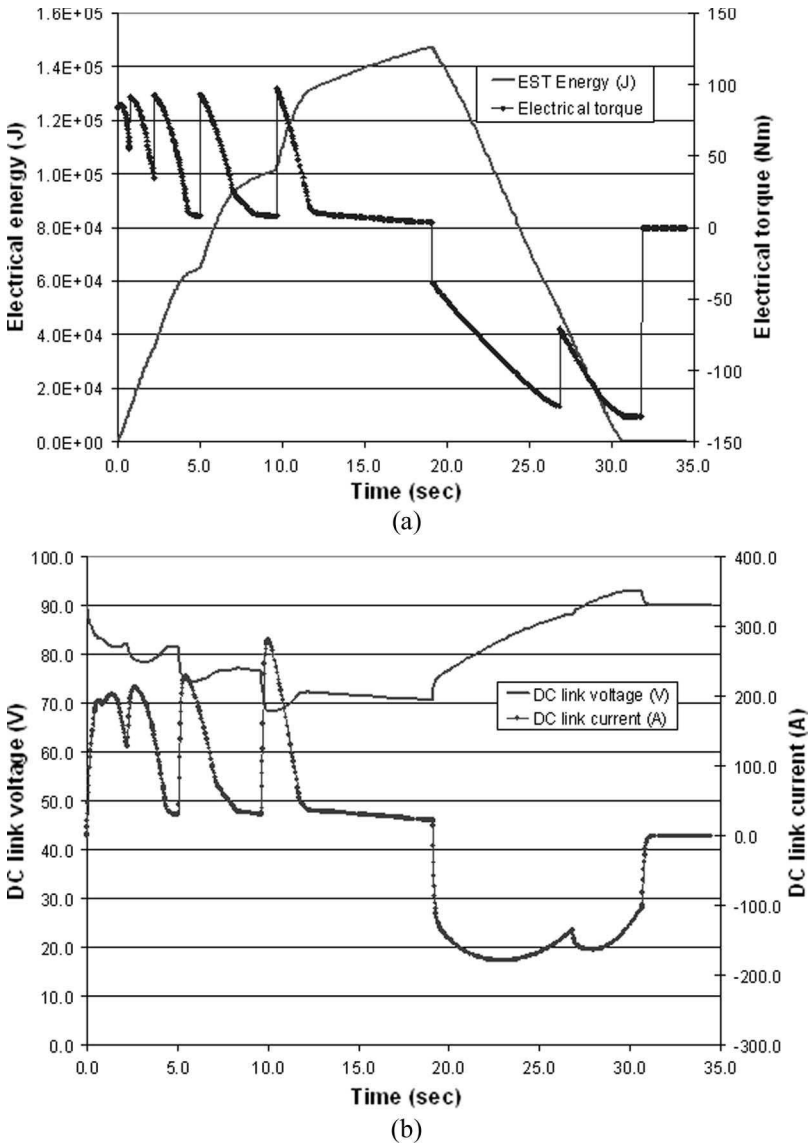

Fig. 4. Variation of torque, energy, and supercapacitor voltage and current as functions of time over the reference driving cycle. (a) Torque and energy. (b) Supercapacitor bank voltage and current.

TABLE I
VEHICLE DATA

Front area (m^2)	1.75	Gross weight (kg)	1570
Drag coefficient	0.31	Rolling resistance coefficient	0.009
Wheel radius (m)	0.274	Top speed (km/h)	240

recovered via regeneration during the braking period, as the required energy at the end of the reference driving cycle is zero. This indicates the fact that the energy used for electrical torque boosting during the acceleration period can be fully recovered through regenerative operation during braking, and consequently, the net energy consumption is zero. The rms torque over the driving cycle is ~ 70 N · m, which equates to $\sim$50% of the peak torque requirement. Therefore, if the electrical machine is designed on the basis of a 50% duty ratio with respect to its peak torque capability, the driving cycle can be repeated continuously. Simulations have also been undertaken, assuming the energy-storage unit to have 30 supercapacitors. However, although the energy consumption is similar to that with 36 supercapacitors, the minimum dc-link voltage is significantly lower, and the peak and rms motor currents are much higher, which impacts on the efficiency and thermal behavior of all the power components in the system, particularly the supercapacitors, whose maximum temperature is limited to ~ 60 °C.

Simulations have also been carried out for other driving cycles, such as the New European Driving Cycle (NEDC), in order to quantify the energy consumption and torque requirements. However, the acceleration requirement can, in most cases, be met by the 1.8l TC downsized ICE engine. On the other hand, the electrical torque booster may still be used to reduce CO_2 emissions in urban areas, to recover braking energy, or to improve the overall efficiency or response time of the vehicle power train. Under these circumstances, a suitable torque-sharing strategy between the ICE and the electrical machine and an appropriate energy-management strategy for the supercapacitors are essential [7], [8]. The control can be

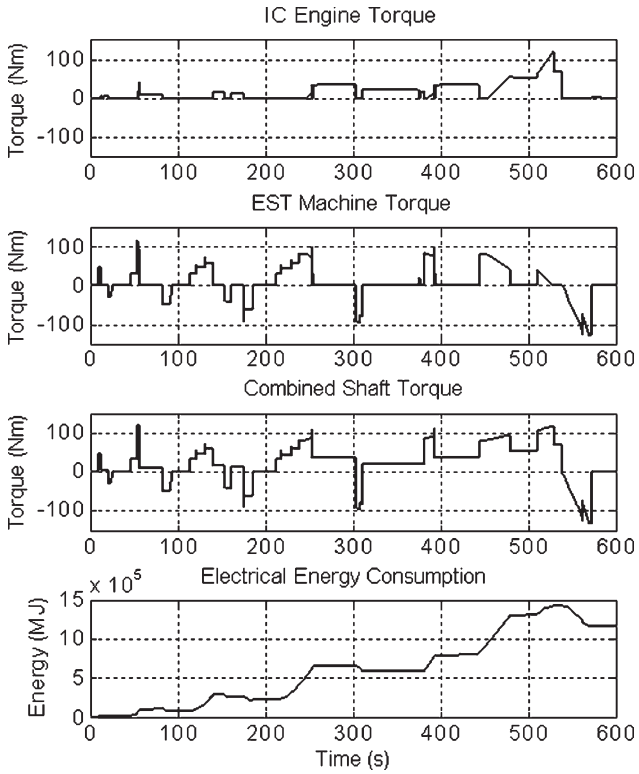

Fig. 5. Variations of torque and energy as functions of time over the NEDC cycle.

optimized according to the main objectives, such as energy consumption and acceleration behavior, in order to achieve the following:

1) ensure drivability;
2) minimize fuel consumption;
3) minimize toxic emission;
4) ensure the durability of engine/electrical torque-boost components;
5) minimize noise level.

Unfortunately, these objectives are, to some extent, mutually exclusive, so that they need to be weighted and evaluated. For example, running the electric motor over a long period initially allows pollution-free driving but depletes the stored electric energy in the medium term. Thus, reducing pollutants and fuel consumption cannot be the sole focus of the control- and energy-management strategy. Furthermore, evaluation of the weighted optimum is sometimes subjective and, in any case, must be based on the availability of a reliable characteristic data of the electric torque-boosting system, which will be described in the subsequent sections.

By way of example, Fig. 5 shows the variation of the total traction torque, the ICE torque, and the electrical machine torque as functions of time over the NEDC cycle, assuming that the torque booster provides its maximum torque when the vehicle is accelerating and regenerates energy during braking, according to the torque–speed characteristic defined in Fig. 1, together with the corresponding electrical-energy consumption. As shown, although the rms electrical torque over the NEDC cycle under this strategy is < 40 N $\cdot$ m, i.e., $< 50\%$ of the peak torque capability, the total energy consumption is 1.2 MJ, which

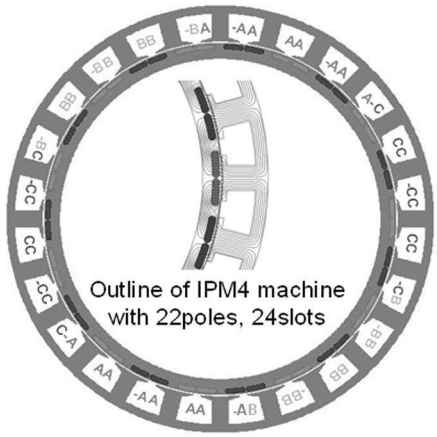

Fig. 6. Modular permanent-magnet brushless machine with 22 poles and 24 slots.

is much greater than the energy-storage capacity of the supercapacitors, even with 585 kJ of energy, which is recovered during regenerative braking. Thus, either the contribution of the torque booster must be reduced, additional energy must be regenerated during the constant speed regions, or the supercapacitor must be recharged by the dc/dc converter. In any case, the balance of energy has to be carefully managed in terms of performance, energy efficiency, and CO_2 emissions.

III. Torque-Boost Machine

Due to constraints imposed by the engine–clutch arrangement, the torque-boost machine must be accommodated within an annular space envelope, which favors a high-pole-number permanent-magnet machine. Although relatively conventional topologies of three-phase permanent-magnet brushless machines [9] having one-slot/pole–pair/phase and either a surface-mounted magnet or an interior-magnet rotor, e.g., 24-poles/36-slots, were designed, the preferred topology combined a stator having a modular three-phase winding [10], in which the coils of each phase are wound on adjacent teeth, with an interior-magnet rotor, viz. 22-poles/24-slots, since this improves the containment of the magnets and introduces a saliency torque component, which, in turn, makes it possible to reduce the back electromotive force (EMF), and, hence, the iron loss and inverter voltage rating, whereas the modular stator winding reduces the likelihood of an interphase fault and is conducive to a high packing factor [11]. Furthermore, it results in a smaller number of slots for a given number of poles, which simplifies manufacture, as well as a fractional number of slots per pole, which is conducive to a low cogging torque. Fig. 6 shows a cross section of the modular permanent-magnet torque-boost machine. Figs. 7–9 compare predicted and measured back-EMF waveforms and electromagnetic torque–current and machine-efficiency-output power characteristics, the demonstrator machine being shown in Fig. 10 on a dynamometer test rig. As shown, the machine exhibits a linear torque–current control characteristic, albeit the measured motor efficiency is slightly lower than that of the prediction. This may be due to the fact that the resistance of the connection leads was not taken into account in the prediction.

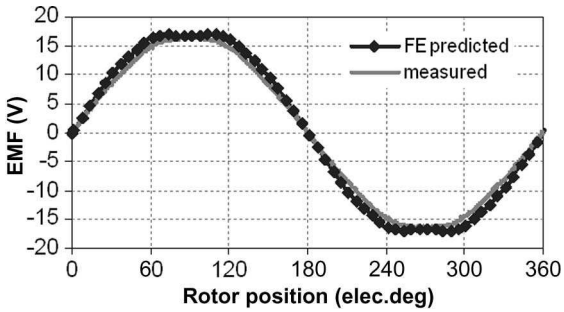

Fig. 7. Comparison of measured and predicted EMF (1000 r/min).

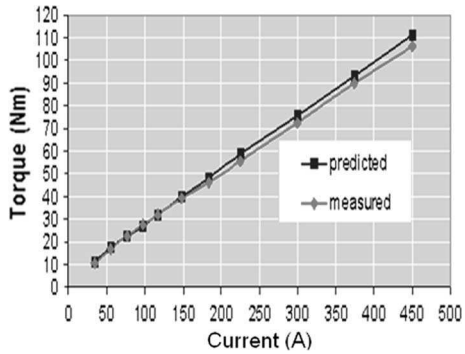

Fig. 8. Comparison of measured and predicted torque–current characteristic (1000 r/min).

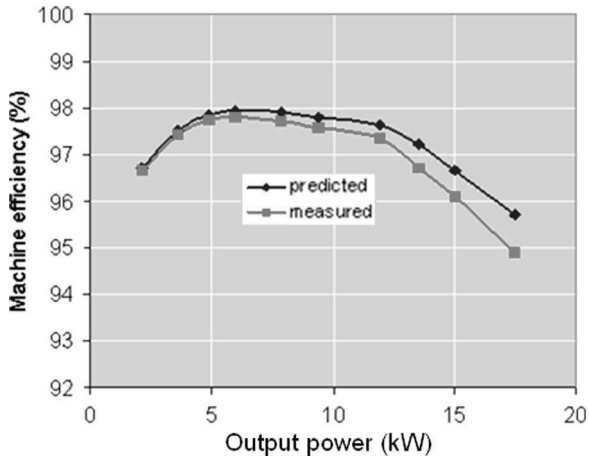

Fig. 9. Comparison of measured and predicted efficiency-power characteristics.

IV. Experimental Characterization

Fig. 11 shows a schematic of the electric torque-boost test system, on which initial tests were performed with a four-quadrant dc power supply, which was subsequently replaced by the supercapacitor unit. The torque-boost machine operates in brushless ac mode, and its torque equation is

$$T = (3p/2)\left[\psi_f I_q + (L_d - L_q) I_d I_q\right] \tag{1}$$

where p is the number of pole-pairs; ψ_f is the flux-linkage due to permanent magnets; and I_d, I_q and L_d, L_q are the d- and

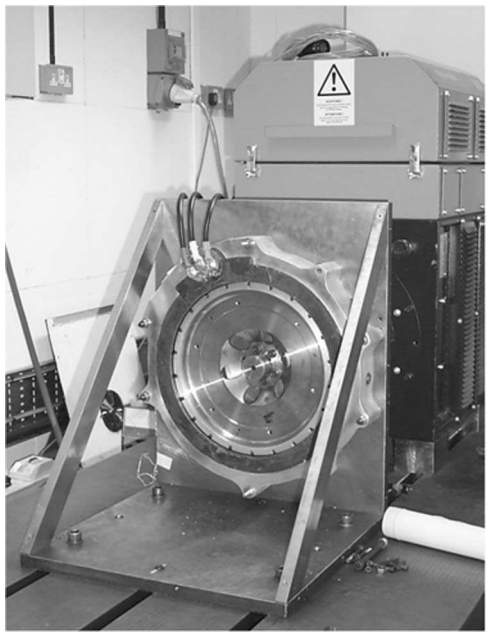

Fig. 10. Demonstrator torque-boost machine on dynamometer test rig.

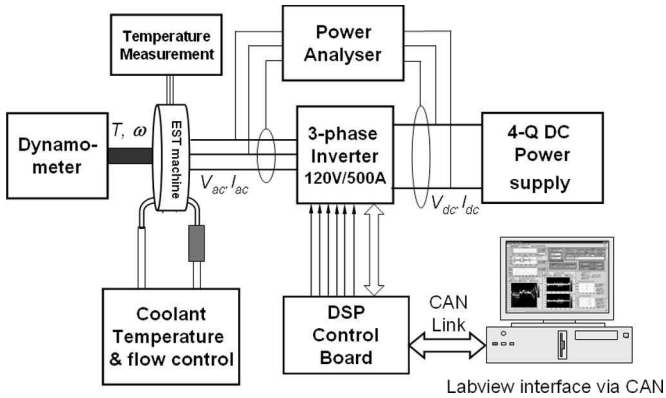

Fig. 11. Torque-boost test system.

q-axis currents and inductances, respectively. Thus, below base-speed, when the dc-bus voltage provided by the supercapacitors is sufficient to produce the current which is required to meet the torque demand, I_d is set to zero, and the torque is proportional to I_q, the required value being given by the following: $I_q^* = 2T_{\rm den}/3p\psi_f$, where $T_{\rm den}$ is the demanded torque. Above base-speed, when the back EMF is higher than the dc-bus voltage which can be provided by the supercapacitors, flux-weakening control is employed by applying a negative d-axis of I_d. However, since the dc bus is variable when it is supplied from a supercapacitor unit, the base-speed is also variable, and the optimal flux-weakening vector-control algorithm is implemented in real-time.

The rotor electrical position of the machine is estimated by a hybrid position observer [12] from the three commutation signals used for brushless dc operation. However, the $d-q$-axis transformations used in the ac-control algorithm do not require absolute rotor electrical position but do require its sine and cosine. The hybrid observer algorithm, as shown in Fig. 12, is

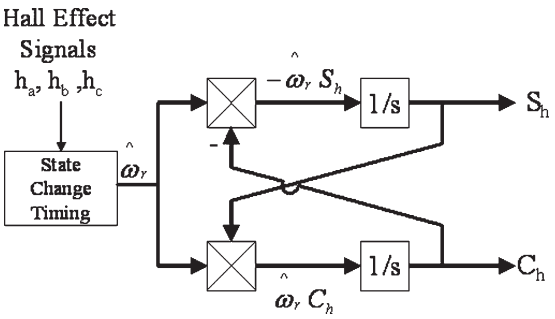

Fig. 12. Schematic of hybrid position observer.

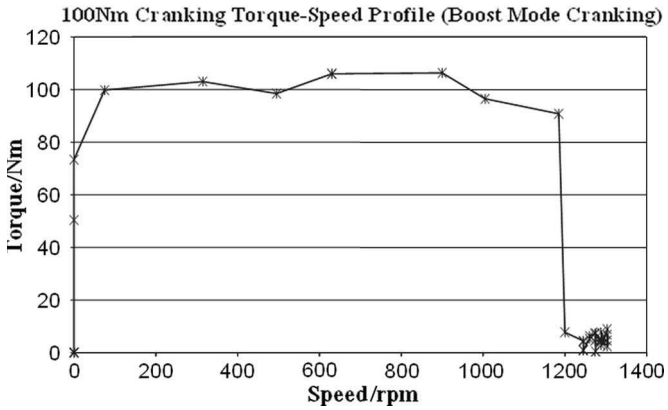

Fig. 13. Cranking test at 100 N · m.

based on the relationship between the integrals of the sine and cosine of an electrical angle, as shown in

$$\int -\omega_{\text{elec}} \sin(\omega_{\text{elec}} t)dt = \cos(\omega_{\text{elec}} t)$$
$$\int \omega_{\text{elec}} \cos(\omega_{\text{elec}} t)dt = \sin(\omega_{\text{elec}} t). \quad (2)$$

This relationship is implemented by two integrators: one to calculate the sine and the cosine. The integrators are seeded with an initial value at each transition point of the commutation signals, and the maximum and minimum values of the integrators are bounded, for the sector in question, to minimize the error output of the algorithm. The electrical rotational speed of the rotor is calculated from the time interval between two commutation transitions using the internal DSP timer, where the minimum operating speed, at which the observer algorithm is stable, is limited by the DSP-timer overflow period.

A. Cranking Mode

Fig. 13 shows the result of a cranking test in which the electrical machine was required to overcome a static torque of 100 N · m and maintain it dynamically until the point where the ICE should have started. It will be noted that 100 N · m was a limit imposed by the dynamometer and that the machine was operated in brushless ac mode.

B. Torque-Boost Mode

In order to demonstrate the torque-boosting and regeneration capability of the system, the torque demand was repeatedly reversed with the speed held constant by the dynamometer.

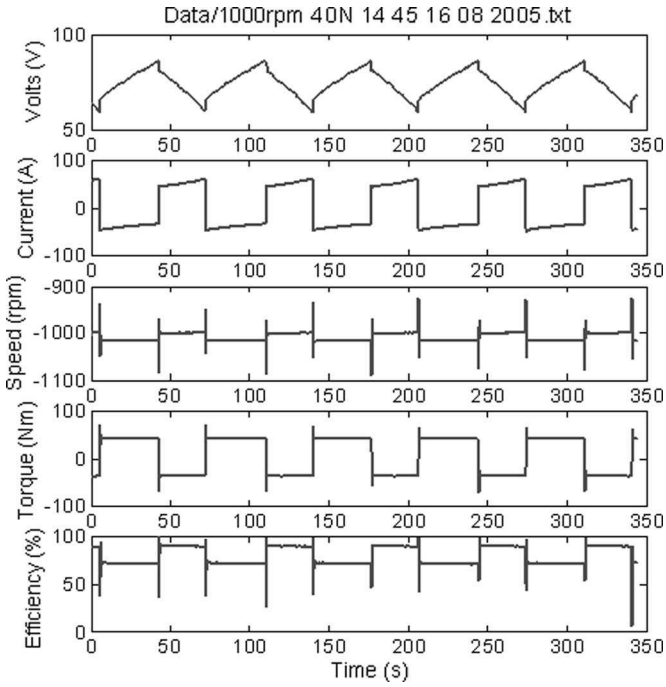

Fig. 14. Voltage, current, torque, and efficiency waveforms of torque-boost system (±40 N · m, 1000 r/min).

Thus, energy was cycled into and out of the supercapacitors, and the net input energy was zero. The test was repeated at different speeds and torques encompassing the full operating range required of the system. However, due to the maximum torque limit of the dynamometer, tests could only be performed up to 100 N · m. Fig. 14 shows a typical test result at 1000 r/min and ±40 N · m. It consists of a period during which the machine generates and charges the supercapacitors until their terminal voltages reach a preset value of 90 V. The mode of operation then reverses and the machine operates in torque-boosting mode when the supercapacitors discharge until their terminal voltage decreases to a preset value of 60 V and when the entire cycle is repeated. The average efficiencies of the machine and inverter η_{mi}, the supercapacitor unit η_{sc}, and the complete torque-boost system η may be evaluated from

$$\eta_{\text{mi}} = \frac{1}{2}\left\{\frac{\int_{T_c} \nu_{\text{dc}}(t) i_{\text{dc}}(t)dt}{\int_{T_c} \omega(t)T(t)dt} + \frac{\int_{T_d} \omega(t)T(t)dt}{\int_{T_d} \nu_{\text{dc}}(t) i_{\text{dc}}(t)dt}\right\}$$
$$\eta_{\text{sc}} = \frac{\int_{T_d} \nu_{\text{dc}}(t) i_{\text{dc}}(t)dt}{\int_{T_c} \nu_{\text{dc}}(t) i_{\text{dc}}(t)dt}$$
$$\eta = \frac{\int_{T_d} \omega(t)T(t)dt}{\int_{T_c} \omega(t)T(t)dt}. \quad (3)$$

By way of example, Figs. 15–17 show the measured efficiency maps of the supercapacitor bank, the machine and inverter subsystem, and the electric torque-boost system over the full torque–speed operating range, respectively. Each rectangular box represents a particular operation condition (speed and torque) under which a repeated cycling test was performed. As shown, there are a few blank boxes in the maps due to the relevant data being either not available or corrupted.

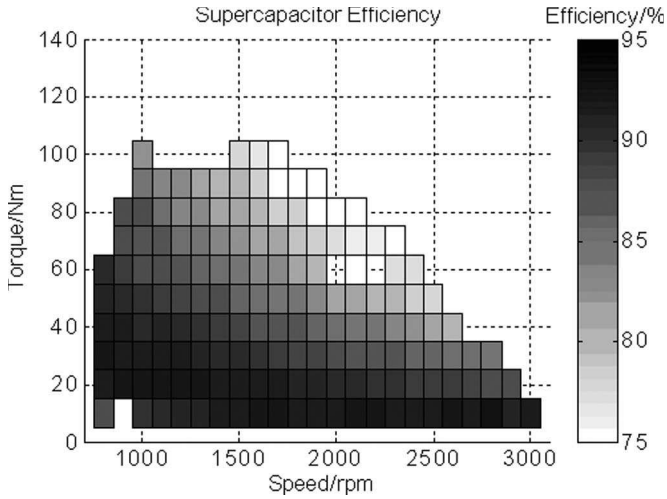

Fig. 15. Efficiency map of the supercapacitor unit.

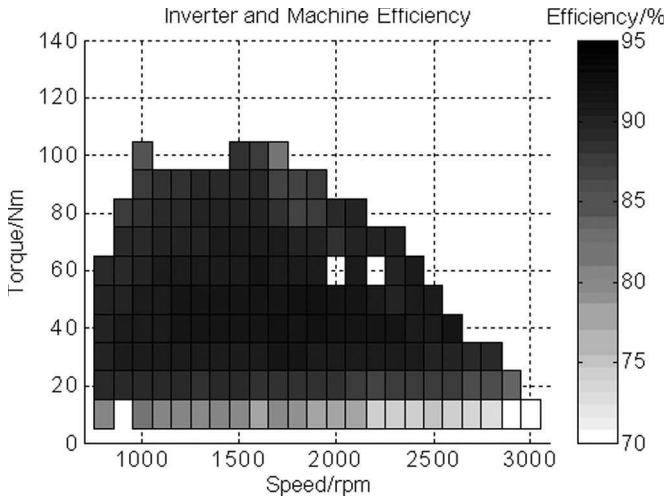

Fig. 16. Efficiency map of the torque-boost machine and inverter.

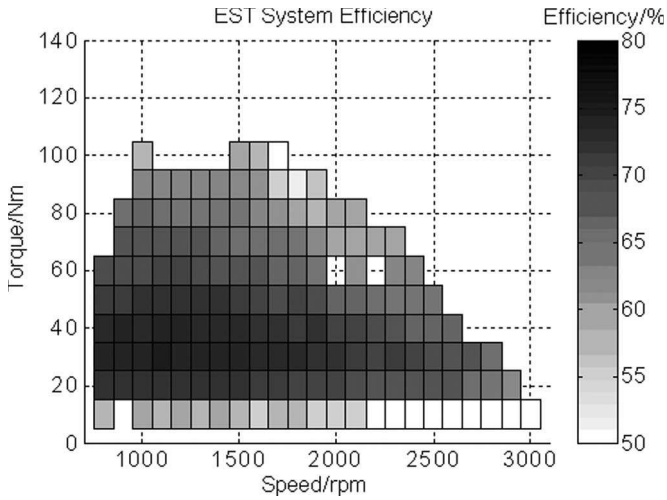

Fig. 17. Efficiency map of the torque-boost system.

The measured machine- and inverter-subsystem efficiency is consistent with the separately measured torque-boost machine shown in Fig. 9. From these data, it can be inferred that the inverter efficiency is around 95% at its rated operating point. It can also be observed that the torque-boost system operate most efficiently within the medium power range, i.e., speed between 1000 and 2000 r/min and torque between 30 and 60 N · m.

V. Conclusion

A torque-boost system for use with a downsized ICE has been described. It combines an interior-magnet brushless ac machine and a supercapacitor energy-storage buffer and facilitates regenerative energy recovery and cranking of the engine. The operations of the system have been experimentally characterized. It has been shown that the overall system-cycle efficiency (torque boosting and regenerative braking) is around 70%, and the torque-boost system operates most efficiently within the medium power range, i.e., 1000–2000 r/min and 30–60 N · m.

References

[1] H. Kahlen and G. Maggetto, "Electric and hybrid vehicles," in *Proc. EPE*, Trondheim, Norway, 1997, pp. 1030–1054.
[2] C. C. Chan, "The state of the art of electric and hybrid vehicles," *Proc. IEEE*, vol. 90, no. 2, pp. 247–275, Feb. 2002.
[3] J. M. Miller, A. Emadi, A. V. Rajarathnam, and M. Ehsani, "Current status and future trends in more electric car power systems," in *Proc. IEEE Veh. Technol. Conf.*, Houston, TX, May 1999, pp. 1380–1384.
[4] S. Barsali, C. Miulli, and A. Possenti, "A control strategy to minimize fuel consumption of series hybrid electric vehicles," *IEEE Trans. Energy Convers.*, vol. 19, no. 1, pp. 187–195, Mar. 2004.
[5] S. M. Lukic and A. Emadi, "Effects of drivetrain hybridization on fuel economy and dynamic performance of parallel hybrid electric vehicles," *IEEE Trans. Veh. Technol.*, vol. 53, no. 2, pp. 385–389, Mar. 2004.
[6] J. Wang, Z. P. Xia, B. Taylor, and D. Howe, "Supercapacitor-based torque booster for down-sized ICE vehicle," in *Proc. PEMD*, Edinburgh, U.K., Mar. 31–Apr. 2, 2004, pp. 55–60.
[7] R. M. Schupbach and J. C. Baldo, "The role of ultra capacitors in an energy storage unit for vehicle power management," in *Proc. IEEE VTC—Fall*, Oct. 6–9, 2003, pp. 3236–3240.
[8] J. M. Miller and R. Smith, "Ultra-capacitor assisted electric drives for transportation," in *Proc. Int. Elect. Mach. Drives Conf.*, Madison, WI, Jun. 1–4, 2003, pp. 670–676.
[9] J. R. Hendershot, Jr. and T. J. E. Miller, "Electrical design," *Design of Brushless Permanent-Magnet Motors.* Hillboro, OH: Magna Phys., 1994, ch. 5, pp. 5555–561.
[10] K. Atallah, J. Wang, and D. Howe, "Torque ripple minimization in modular permanent magnet brushless machines," *IEEE Trans. Ind. Appl.*, vol. 36, no. 6, pp. 1689–1695, Nov./Dec. 2003.
[11] J. Wang, Z. P. Xia, and D. Howe, "Three-phase modular permanent magnet brushless Machine for torque boosting on a downsized ICE vehicle," *IEEE Trans. Veh. Technol.*, vol. 54, no. 3, pp. 809–816, May 2005.
[12] K. A. Corzine and S. D. Sudhoff, "A hybrid observer for high performance brushless DC motor drives," *IEEE Trans. Energy Convers.*, vol. 11, no. 2, pp. 318–323, Jun. 1996.

Jiabin Wang (SM'03) received the B.Eng. and M.Eng. degrees in electrical and electronic engineering from Jiangsu University of Science and Technology, Zhengjiang, China, in 1982 and 1986, respectively, and the Ph.D. degree in electrical and electronic engineering from the University of East London, London, U.K., in 1996.

From 1986 to 1991, he was with the Department of Electrical Engineering, Jiangsu University of Science and Technology, where he was appointed a Lecturer in 1987 and an Associated Professor in 1990. He was a Postdoctoral Research Associate with the University of Sheffield, Sheffield, U.K., from 1996 to 1997, and a Senior Lecturer with the University of East London from 1998 to 2001. He is currently a Reader in electrical engineering with the Department of Electronic and Electrical Engineering, University of Sheffield. His research interests range from motion control to electromagnetic devices and their associated drives.

Ben Taylor received the M.Eng. degree in electronic engineering (communications) from the University of Sheffield, Sheffield, U.K., in 1998.

He is currently a Research Associate with the University of Sheffield, working on power electronics and control systems for novel gasoline combustion engines and energy scavenging from energy-sparse environments.

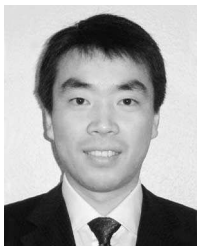

Zhigang Sun received the B.Eng. and M.Eng. degrees in electrical and electronic engineering from Shanghai Jiao Tong University, Shanghai, China, in 2001 and 2004, respectively. He is currently working toward the Ph.D. degree with the Electrical Machines and Drives Research Group, University of Sheffield, Sheffield, U.K.

From 2004 to 2005, he became a Visiting Researcher with the Electrical Machines and Drives Research Group, University of Sheffield. His research topic is in control of fault-tolerant permanent-magnet machines, which is funded by the Rolls-Royce University Technology Center, University of Sheffield. His research interests include control of permanent-magnet machines and power-electronic drives.

David Howe received the B.Tech. and M.Sc. degrees in electrical power engineering from the University of Bradford, Bradford, U.K., in 1966 and 1967, respectively, and the Ph.D. degree in electrical power engineering from the University of Southampton, Southampton, U.K.

He has held academic posts at Brunel University, London, U.K., and at the University of Southampton and spent a period in industry with NEI Parsons Ltd., Newcastle-Upon-Tyne, U.K., working on electromagnetic problems related to turbogenerators. He is currently a Professor of electrical engineering with the University of Sheffield, Sheffield, U.K., where he heads the Electrical Machines and Drives Research Group. His research activities span all facets of controlled electrical-drive systems, with particular emphasis on permanent-magnet-excited machines.

Dr. Howe is a Fellow of the Institution of Electrical Engineers, U.K., and the Royal Academy of Engineering, U.K.